

This discussion paper is/has been under review for the journal Hydrology and Earth System Sciences (HESS). Please refer to the corresponding final paper in HESS if available.

Improving the snow physics of WEB-DHM and its point evaluation at two SnowMIP alpine sites

M. Shrestha¹, L. Wang¹, T. Koike¹, Y. Xue², and Y. Hirabayashi³

¹Dept. of Civil Engineering, The University of Tokyo, Tokyo, Japan

²Dept. of Geography, University of California, Los Angeles, USA

³Institute of Engineering Innovation, The University of Tokyo, Tokyo, Japan

Received: 25 May 2010 – Accepted: 28 May 2010 – Published: 15 June 2010

Correspondence to: M. Shrestha (maheswor@hydra.t.u-tokyo.ac.jp)

Published by Copernicus Publications on behalf of the European Geosciences Union.

HESSD

7, 3481–3519, 2010

Improving the snow physics

M. Shrestha et al.

Title Page

Abstract

Introduction

Conclusions

References

Tables

Figures

◀

▶

◀

▶

Back

Close

Full Screen / Esc

Printer-friendly Version

Interactive Discussion



Abstract

The snow physics of a distributed biosphere hydrological model, referred to as the Water and Energy Budget based Distributed Hydrological Model (WEB-DHM) is improved by incorporating the three-layer physically based energy balance snowmelt model of Simplified Simple Biosphere 3 (SSiB3) and the Biosphere-Atmosphere Transfer Scheme (BATS) albedo scheme. WEB-DHM with improved snow physics (WEB-DHM-S) can simulate the variability of snow density, snow depth and snow water equivalent, liquid water and ice content in each layer, prognostic snow albedo, diurnal variation in snow surface temperature, thermal heat due to conduction and liquid water retention. The performance of WEB-DHM-S is evaluated at two alpine sites of the Snow Model Intercomparison Project with different climate characteristics: Col de Porte in France and Weissfluhjoch in Switzerland. The simulation results of the snow depth, snow water equivalent, surface temperature, snow albedo and snowmelt runoff reveal that WEB-DHM-S is capable of simulating the internal snow process better than the original WEB-DHM, with the root mean square error and bias error being remarkably reduced. Although WEB-DHM-S is only evaluated at a point scale for the simulation of snow processes, this study provides a benchmark for the application of WEB-DHM-S in cold regions in the assessment of the basin-scale snow water equivalent and seasonal discharge simulation for water resources management.

1 Introduction

Seasonal snow cover is an important component of land surface hydrology and is critical for simulation of water and energy budgets in cold climate regions. Snow with its high albedo, low roughness, relatively low thermal conductivity and considerable spatial and temporal variability, can greatly alter energy and water interactions among the atmosphere, vegetation and land. Snow has the ability to store and release water within the hydrological cycle. The appearance of snow cover may lead to a temporal

HESSD

7, 3481–3519, 2010

Improving the snow physics

M. Shrestha et al.

Title Page

Abstract

Introduction

Conclusions

References

Tables

Figures

◀

▶

◀

▶

Back

Close

Full Screen / Esc

Printer-friendly Version

Interactive Discussion



shift in the runoff during the spring snowmelt period and is a significant parameter from the view of hydrological simulation.

To understand and represent the snow processes in land surface modeling, a large number of approaches have been used in many land surface schemes in diversified numerical expressions, ranging from simple degree-day models to physically based sophisticated multi-layer energy balance models. Many numerical studies have been carried out to develop and validate snow submodels of different complexity in land surface schemes of many climate and hydrological models (e.g., Versegny, 1991; Blöschl et al., 1991; Douville et al., 1995; Tarboton and Luce, 1996; Yang et al., 1997; Loth and Graf, 1998a,b; Marks et al., 1999; Jin et al., 1999a,b; Sun et al., 1999; Sud and Mocko, 1999; Essery et al., 1999; Smirnova et al., 2000; Mocko and Sud, 2001; Sun and Xue, 2001; Xue et al., 2003; Yang and Niu, 2003; Dai et al., 2003; Zanotti et al., 2004; Sun and Chern, 2005; Liston and Elder, 2006; Hirai et al., 2007). Several snow-scheme inter-comparison studies have been undertaken to gain an improved understanding of snow cover simulation in land surface schemes and to address issues related to the current state of snow modeling used by the atmospheric and hydrologic research community (e.g., the Project for the Intercomparison of Land-Surface Parameterization Schemes (PILPS) – Phase 2d (Slater et al., 2001) and Phase 2e (Bowling et al., 2003), the Snow Model Intercomparison Project (SnowMIP) – Phase 1 (Etchevers et al., 2004) and Phase 2 (Rutter et al., 2009; Essery et al., 2009) and the Rhône-Aggregation Land Surface Scheme Intercomparison Project (Boone et al., 2004)). Many studies showed that the performances of simple snow models are good in snow accumulation simulations but these models cannot capture the real snow physics to represent diurnal freeze and thaw cycles, resulting in errors in the simulation of snow surface temperature and snow melting in terms of timing and the total amount (Lynch-Stieglitz, 1994; Sun et al., 1999, Jin et al., 1999b; Slater et al., 2001; Luo et al., 2003; Xue et al., 2003), raising the importance of the development and application of multilayer energy-balance-based snow models.

Improving the snow physics

M. Shrestha et al.

Title Page

Abstract

Introduction

Conclusions

References

Tables

Figures

◀

▶

◀

▶

Back

Close

Full Screen / Esc

Printer-friendly Version

Interactive Discussion



Improving the snow physics

M. Shrestha et al.

Title Page

Abstract

Introduction

Conclusions

References

Tables

Figures

I◀

▶I

◀

▶

Back

Close

Full Screen / Esc

Printer-friendly Version

Interactive Discussion



Although snow parameterization was carried out employing multilayer energy-balance-based snow models in many land surface schemes, no such model has been employed in distributed biosphere hydrological models for snow process simulations. Water and Energy Budget based Distributed Hydrological Model (WEB-DHM; Wang et al., 2009a, b, c) is a distributed biosphere hydrological model, developed by fully coupling Simple Biosphere 2 (SiB2; Sellers et al., 1996) with a Geomorphology Based Hydrological Model (GBHM; Yang et al., 2002, 2004). It can realistically simulate the land surface and hydrological processes and provide consistent descriptions of water, energy and CO₂ fluxes at a basin scale. This study attempts to improve the simple snow physics of WEB-DHM by adopting many ideas derived from the studies of different snow models and by incorporating the three-layer snow physics of Simplified Simple Biosphere 3 (SSiB3; Sun and Xue, 2001; Xue et al., 2003). SSiB3 was developed by coupling SSiB (Xue et al., 1991) with a three-layer version of the Simple Atmosphere-Snow Transfer (SAST; Sun et al., 1999) and has been successfully applied to simulate snow processes in cold regions (Xue et al., 2003; Durand and Margulis, 2006; Walisher et al., 2009).

This paper discusses the improvement in the snow physics of WEB-DHM and its evaluation at a point scale using observational datasets from two alpine sites of the SnowMIP project: Col de Porte in the French Alps and Weissfluhjoch in the Swiss Alps. WEB-DHM with improved snow physics is hereafter termed WEB-DHM-S.

2 Model description

A short review of the snow processes in WEB-DHM is given in Sect. 2.1, while the snow processes in WEB-DHM-S are discussed in detail in Sect. 2.2. Details of the hydrological and land surface submodels of WEB-DHM can be found in Wang et al. (2009a) and Sellers et al. (1996).

2.1 Snow processes in WEB-DHM

In WEB-DHM, the parameterization of the snow submodel is the same as that for SiB2 (Sellers et al., 1996). A single-layer bulk snow mass balance is considered with constant density (200 kg m^{-3}), and the thermal regime of snow is not distinguished from that of soil. Attenuation of downward shortwave radiation through the canopy is considered with multiple scattering between the canopy and snow/ground but attenuation of radiation within the snow layer is ignored. Only the top 5 cm of the snow water equivalent is considered for variation of the heat capacity of the surface skin, which affects the surface energy balance in the case of a large snow mass. The snow surface temperature is represented by the average snowpack temperature, which tends to result in incorrect simulation of the surface energy budget, which in turn affects the overall accumulation and melting processes. Moreover, it does not consider the prognostic snow albedo. The dry snow albedo is given as a constant value of 0.8 for visible (VIS) shortwave radiation and 0.4 for near infrared (NIR) shortwave radiation. For melting snow, the snow albedo is simply set to 60% of the dry snow albedo.

2.2 Snow processes in WEB-DHM-S

In this section, the energy and mass budget equations along with snow parameterization are presented in detail. In WEB-DHM-S, the snow parameterizations for the canopy are kept the same as in WEB-DHM, but the single-layer snow scheme on the ground is replaced by the SSiB3 snow scheme when the snow depth is greater than 5 cm. Initially, the snowpack is divided into three layers that start with the same initial snow temperatures. The top layer thickness is kept at a fixed depth of 2 cm regardless of the total snow depth to provide reasonable simulation of the diurnal changes in the snow surface temperature. The maximum thickness of the middle layer is kept at 20 cm, and the bottom layer represents the remaining body of the snowpack. A surface energy balance equation is formulated only for the top layer, which is influenced by the surface radiation budget and sensible and latent heat fluxes. The heat budget of

HESSD

7, 3481–3519, 2010

Improving the snow physics

M. Shrestha et al.

Title Page

Abstract

Introduction

Conclusions

References

Tables

Figures

◀

▶

◀

▶

Back

Close

Full Screen / Esc

Printer-friendly Version

Interactive Discussion



the second and third layers is controlled by the heat conduction and the penetrating shortwave radiation. Over time, these three layers evolve differently through their own energy budgets and the heat exchanges between them.

Meanwhile, the mass budget for each layer is calculated accordingly by taking account of the precipitation, evaporation/condensation, compaction, liquid water retention, snowmelt runoff and infiltration into the underlying layers. When snow melts, meltwater in a layer increases, thereby increasing the layer-average density and mass. Any meltwater in a layer exceeding the liquid water holding capacity is delivered to the underlying layer. Water leaving the bottom snow layer is available for partitioning into soil water infiltration and/or surface runoff by the soil-vegetation-atmosphere transfer (SVAT) system. This snow scheme can produce a variable density profile.

The snow-covered surface albedo scheme is parameterized using a physically based prognostic snow albedo scheme of the Biosphere-Atmosphere Transfer Scheme (BATS) model (Dickinson et al., 1993; Yang et al., 1997), and the snow cover fraction is calculated using the formulations of Mocko and Sud (2001). Major differences between the snow processes in WEB-DHM and WEB-DHM-S are presented in Table 1. The soil model coupled with a three layer snow model in WEB-DHM-S is shown in Fig. 1.

2.2.1 Snow layer subdivision

The number of snow layers for this model is fixed at three, which is considered to be adequate to resolve the snow thermal profile between the top and base of the snow cover (Sun et al., 1999; Jin et al., 1999b; Sun and Xue, 2001; Boone and Etchevers, 2001). When the total snow depth is more than 5 cm, WEB-DHM-S will be adopted; otherwise WEB-DHM will be employed for simulation. The method of layering the snowpack is discussed here. When the snow depth is between 5 and 8 cm, the top and middle layer thicknesses are fixed at 2 cm and the thickness of the bottom layer is the total snow depth minus the top and middle layer thickness. When the snow depth is between 8 and 62 cm, the top layer thickness is kept at 2 cm, the middle layer thickness is 33% of the total snow depth minus the surface layer thickness so that the middle layer

Improving the snow physics

M. Shrestha et al.

Title Page

Abstract

Introduction

Conclusions

References

Tables

Figures

◀

▶

◀

▶

Back

Close

Full Screen / Esc

Printer-friendly Version

Interactive Discussion



thickness is limited to 20 cm, and the residual is taken as the bottom layer thickness. When the snow depth is more than 62 cm, the surface and middle layer thickness are fixed at 2 and 20 cm, respectively and the residual is taken as the bottom layer thickness. This layering scheme can achieve reasonable simulations of diurnal changes in surface temperature, heat conduction between snowpack layers and interaction of the bottom snow layer with soil. The mass and energy is redistributed while dividing the snow layers after execution of one time step of the model and this is followed by either accumulation or melting.

2.2.2 Energy balance equations

The energy content of the snowpack is affected by the shortwave radiation penetration, heat conduction between sublayers, ground heat fluxes, the flux of advection due to precipitation, energy due to phase change and net radiation at the surface accompanied by sensible and latent heat fluxes. Specific enthalpy is used as the prognostic variable instead of snow temperature in the energy balance equation, which includes the internal energy of liquid water or ice as well as the energy of the phase change. It is assumed that liquid water at its melting point has zero enthalpy so that the phase change processes can be tackled easily. The same approach was also employed by Lynch-Stieglitz (1994), Tarboton and Luce (1996), Jin et al. (1999a), Sun et al. (1999) and Sun and Xue (2001). The energy budget equation for the canopy is the same as that in WEB-DHM. However, the canopy temperature is influenced by the snow surface enthalpy. The energy budget equation for the canopy is

$$C_c \frac{\partial T_c}{\partial t} = R_{nc} - H_c - \lambda E_c - \xi_c, \quad (1)$$

where C_c ($\text{Jm}^{-2}\text{K}^{-1}$) is the effective heat capacity for the canopy, R_{nc} , H_c and λE_c (Wm^{-2}) are net radiation, sensible heat flux and latent heat flux for the canopy, respectively, and ξ_c (Wm^{-2}) is the energy transfer due to phase changes in the canopy. The

Improving the snow physics

M. Shrestha et al.

Title Page

Abstract

Introduction

Conclusions

References

Tables

Figures

◀

▶

◀

▶

Back

Close

Full Screen / Esc

Printer-friendly Version

Interactive Discussion



equation for enthalpy of each snow layer is

$$\frac{\partial H(Z_j)}{\partial t} = -\frac{\partial G_{sn}(Z_j)}{\partial Z}, \quad (2)$$

where H (Jm^{-3}) is the volumetric enthalpy of water, Z_j is the snow depth of layer j and G_{sn} (Wm^{-2}) is the heat flux through the snow layer. H and G_{sn} are defined as

$$H(Z_j) = C_v(Z_j) \times \{T_{sn}(Z_j) - 273.16\} - f_{ice}(Z_j) \times h_v \times \rho_s(Z_j). \quad (3)$$

$$G_{sn}(Z_j) = \begin{cases} R_{nsn} - H_{sn} - \lambda E_{sn} + G_{pr} & \text{at snow surface}(j=3) \\ K(Z_j) \frac{\partial T_{sn}(Z_j)}{\partial Z} + SW_{sn}(Z_j) & \text{within snow layers}(j=2, 1) \end{cases}, \quad (4)$$

where R_{nsn} (Wm^{-2}), H_{sn} (Wm^{-2}), λE_{sn} (Wm^{-2}), G_{pr} (Wm^{-2}), K ($\text{Wm}^{-1}\text{K}^{-1}$), T_{sn} (K) and SW_{sn} (Wm^{-2}) are net radiation, sensible heat, latent heat flux, thermal energy from rain at the snow surface, thermal conductivity of snow, snow temperature and shortwave radiation flux absorbed by the snow layer, respectively. f_{ice} is the dry-snow mass fraction of the total mass in the snow layer, and h_v (J kg^{-1}) is the latent heat of fusion for ice. C_v ($\text{Jm}^{-3}\text{K}^{-1}$) is the mean snow volumetric specific heat capacity, parameterized as a function of the bulk density of snow (ρ_s ; kg m^{-3}) and intrinsic density of ice (ρ_i ; kg m^{-3}) following Verseghy (1991):

$$C_v = 1.9 \times 10^6 \frac{\rho_s}{\rho_i}. \quad (5)$$

The thermal conductivity of snow K ($\text{Wm}^{-1}\text{K}^{-1}$) is adopted from Jordan (1991).

$$K = K_a + \left(7.75 \times 10^{-5} \rho_s + 1.105 \times 10^{-6} \rho_s^2\right) \times (K_i - K_a), \quad (6)$$

where K_i ($2.29 \text{Wm}^{-1}\text{K}^{-1}$) and K_a ($0.023 \text{Wm}^{-1}\text{K}^{-1}$) are the thermal conductivities of ice and air, respectively. The penetration of shortwave radiation flux into the snow

layers is accounted for in this model. Hence, the shortwave energy available for the surface energy budget is completely different from that in WEB-DHM. The shortwave radiation SW_{sn} at the snow layer is defined following Jordan (1991):

$$SW_{sn}(Z_j) = \begin{cases} SW_{nsn} \times [1 - \exp(-\beta_{vis} \cdot Z_j - 0.002 \cdot \beta_{nir})] & \text{top layer} \\ SW_{nsn} \times [1 - \exp(-\beta_{vis} \cdot Z_j)] \times \exp(-\beta_{vis} \cdot Z_{j+1} - 0.002 \cdot \beta_{nir}) & \text{middle layer} \\ SW_{nsn} \times \exp(-\beta_{vis} \cdot Z_{j+1}) \times \exp(-\beta_{vis} \cdot Z_{j+2} - 0.002 \cdot \beta_{nir}) & \text{bottom layer} \end{cases} \quad (7)$$

where $SW_{nsn} = SW_{sntop}(1 - \alpha_s)$. SW_{sntop} (Wm^{-2}) is the radiation incident on the snow surface, α_s is snow albedo and β_{vis} and β_{nir} are extinction coefficients; $\beta_{vis} = 0.003795d^{-1/2}\rho_s(Z_j)$ and $\beta_{nir} = 400$. The grain size diameter is represented by d (m). The process of the calculations of R_{nsn} , H_{sn} and λE_{sn} is the same as for WEB-DHM except that the snow surface temperature is used instead of the average bulk snow temperature for the surface energy balance. Thermal energy from rain (G_{pr}) can be calculated as

$$G_{pr} = \rho_w \times C_w \times (T_{rain} - 273.16) \times IF_0 \quad (8)$$

where IF_0 (ms^{-1}) is the infiltrated flux rate of rain at the snow surface, T_{rain} (K) is the temperature of rainfall, ρ_w ($kg\ m^{-3}$) and C_w ($J\ kg^{-1}\ K^{-1}$) are the density and specific heat capacity of water. For simplicity, T_{rain} is considered as air temperature. Ground surface temperature (T_g) and deep soil temperature (T_d) are obtained by considering conductive heat flux at the snow/soil interface and the force-restore model (Deardorff, 1978) of the heat balance in the soil surface.

$$C_g \frac{\partial T_g}{\partial t} = -K(Z_1) \frac{\partial T_{sn}(Z_1)}{\partial Z} - \frac{2\pi C_g (T_g - T_d)}{\tau_d} \quad (9)$$

$$C_d \frac{\partial T_d}{\partial t} = \frac{2\pi C_g (T_g - T_d)}{\tau_d \sqrt{365\pi}} \quad (10)$$

Improving the snow physics

M. Shrestha et al.

Title Page

Abstract

Introduction

Conclusions

References

Tables

Figures

◀

▶

◀

▶

Back

Close

Full Screen / Esc

Printer-friendly Version

Interactive Discussion



where C_g and C_d are the effective heat capacity ($\text{Jm}^{-2} \text{K}^{-1}$) for the soil surface and deep soil, τ_d is the day length (s) and $K(Z_1)$ is the effective thermal conductivity at the snow/soil interface.

The prognostic equations of snow surface enthalpy and canopy temperature are solved simultaneously by calculating the temperature increments for the physics time step using an implicit backward numerical scheme. The final equations for solving ΔT_c and $\Delta T_{sn}(Z_3)$ are represented as

$$\left[\frac{C_c}{\Delta t} - \frac{\partial R_{nc}}{\partial T_c} + \frac{\partial H_c}{\partial T_c} + \frac{\partial \lambda E_c}{\partial T_c} \right] \Delta T_c + \left[\frac{\partial H_c}{\partial T_{sn}(Z_3)} + \frac{\partial \lambda E_c}{\partial T_{sn}(Z_3)} - \frac{\partial R_{nc}}{\partial T_{sn}(Z_3)} \right] \Delta T_{sn}(Z_3), \quad (11)$$

$$= (R_{nc} - H_c - \lambda E_c)$$

$$\left[-\frac{\partial R_{nsn}}{\partial T_c} + \frac{\partial H_{sn}}{\partial T_c} + \frac{\partial \lambda E_{sn}}{\partial T_c} \right] \Delta T_c + \left[\frac{C_v \times Z_3}{\Delta t} - \frac{\partial R_{nsn}}{\partial T_{sn}(Z_3)} + \frac{\partial H_{sn}}{\partial T_{sn}(Z_3)} + \frac{\partial \lambda E_{sn}}{\partial T_{sn}(Z_3)} + K_{\text{eff}} \right] \Delta T_{sn}(Z_3)$$

$$= R_{nsn} - H_{sn} - \lambda E_{sn} + G_{pr} - K_{\text{eff}} \times [T_{sn}(Z_3) - T_{sn}(Z_2)] + \frac{Z_3 \times H(Z_3)}{\Delta t}$$

$$- \frac{C_v \times Z_3 \times [T_{sn}(Z_3) - 273.16]}{\Delta t} + \frac{f_{\text{ice}}^{t-\Delta t} \times M_{\text{snow}}^{t-\Delta t}(Z_3) \times h_v \times \rho_w}{\Delta t}, \quad (12)$$

where K_{eff} ($\text{Wm}^{-2} \text{K}^{-1}$) is the effective thermal conductivity of snow between the top and the middle snow layer and M_{snow} (m) is the snow water equivalent (SWE). K_{eff} is defined as

$$K_{\text{eff}} = \frac{2 \times K(Z_3) \times K(Z_2)}{K(Z_3) \times Z_2 + K(Z_2) \times Z_3}. \quad (13)$$

2.2.3 Mass balance equations

The mass balance equation for the canopy is the same as in WEB-DHM. The mass balance for snow is represented by the change in liquid water and ice content in the snowpack. The relative change in snow mass is controlled by snowfall/rainfall, compaction, snow melting, runoff, infiltration into the underlying snow layer/soil and evaporation/sublimation at the snow surface. Neglecting the effect of water vapor diffusion

Improving the snow physics

M. Shrestha et al.

Title Page

Abstract

Introduction

Conclusions

References

Tables

Figures

◀

▶

◀

▶

Back

Close

Full Screen / Esc

Printer-friendly Version

Interactive Discussion



and its phase change to mass distribution, the mass balance equations for the snow layer are

$$\frac{M_{\text{snow},j}}{\partial t} = \begin{cases} P_s + IF_0 - IF_j - R_j - E_{sn} & \text{top layer}(j=3) \\ IF_{j+1} - IF_j - R_j & \text{other layers}(j=2,1) \end{cases} \quad (14)$$

where $M_{\text{snow},j}$ (m) corresponds to the SWE at snow layer j , P_s (ms^{-1}) is the rate of snowfall, IF_j (ms^{-1}) is the actual liquid water infiltration flux at the interfaces, R_j (ms^{-1}) is runoff from the lower interface and E_{sn} (ms^{-1}) is the combined evaporation and sublimation rate. Infiltration of liquid water into the underlying layers is controlled by the liquid water holding capacity and porosity of the snowpack. The liquid water holding capacity (C_r) is taken as a function of the snow layer density following Anderson (1976):

$$C_r = \begin{cases} C_{r\min} & \gamma_i \geq \gamma_e \\ C_{r\min} + (C_{r\max} - C_{r\min}) \frac{\gamma_e - \gamma_i}{\gamma_e} & \gamma_i < \gamma_e \end{cases} \quad (15)$$

where $C_{r\min} = 0.03$, $C_{r\max} = 0.1$, $\gamma_e = 200 \text{ kg m}^{-3}$ and γ_i (kg m^{-3}) is bulk density of ice. The bulk density of ice for new snowfall is calculated following the formulation used in the CROCUS snow model (Brun et al., 1989, 1992):

$$\gamma_i = \max \left\{ \left[109 + 6 \times (T_{\text{air}} - 273.16) + 26 \times \sqrt{u_m} \right], 50 \right\}, \quad (16)$$

where T_{air} is the air temperature (K) and u_m is the wind speed (ms^{-1}).

2.2.4 Snow compaction

Three snow compaction processes, namely destructive metamorphism, densification due to snow overburden and compaction due to snow melting, are included. The compaction process is critically important for the evolution of density and snow depth. The snow depth is decreased by the compaction and is increased by snowfall. These three

Improving the snow physics

M. Shrestha et al.

Title Page

Abstract

Introduction

Conclusions

References

Tables

Figures

◀

▶

◀

▶

Back

Close

Full Screen / Esc

Printer-friendly Version

Interactive Discussion



components of snow compaction are parameterized following Anderson (1976). The empirical equation for destructive metamorphism is

$$\left[\frac{1}{\Delta z} \frac{\partial \Delta z}{\partial t} \right]_{\text{metamorphism}} = -2.778 \times 10^{-6} \times C_3 \times C_4 \times \exp[-0.04 \times (273.16 - T_{sn})]$$

$$C_3 = \begin{cases} \exp[-0.046 \times (\gamma_i - 150)] & \gamma_i > 150 \\ 1 & \gamma_i \leq 150 \end{cases}, \quad (17)$$

$$C_4 = \begin{cases} 1 & \gamma_l = 0 \\ 2 & \gamma_l > 0 \end{cases}$$

where γ_i (kg m^{-3}) and γ_l (kg m^{-3}) are bulk densities of ice and liquid water and C_3 and C_4 are empirical constants. After snow has undergone its initial settling stage, densification due to overburden proceeds at a slower rate. This compaction rate is a function of snow overburden pressure W_s (Nsm^{-2}), such that

$$\left[\frac{1}{\Delta z} \frac{\partial \Delta z}{\partial t} \right]_{\text{overburden}} = - \frac{W_s \times \exp[-C_5 \times (273.16 - T_{sn}) - C_6 \times \rho_i]}{\eta_o}, \quad (18)$$

where η_o ($3.6 \times 10^6 \text{ Nsm}^{-2}$) is the viscosity coefficient, $C_5 = 0.08 \text{ K}^{-1}$ and $C_6 = 0.023 \text{ m}^3 \text{ kg}^{-1}$. The decrease in thickness of the snow sublayer due to melting is estimated as

$$\left[\frac{1}{\Delta z} \frac{\partial \Delta z}{\partial t} \right]_{\text{melt}} = - \frac{dh_i}{h_i}, \quad (19)$$

where h_i is the dry-snow mass in a unit depth and dh_i is the dry-snow mass that melts in the unit depth. Hence, total compaction over one time step is given by

$$\left[\frac{1}{\Delta z} \frac{\partial \Delta z}{\partial t} \right]_{\text{total}} = \left[\frac{1}{\Delta z} \frac{\partial \Delta z}{\partial t} \right]_{\text{metamorphism}} + \left[\frac{1}{\Delta z} \frac{\partial \Delta z}{\partial t} \right]_{\text{overburden}} + \left[\frac{1}{\Delta z} \frac{\partial \Delta z}{\partial t} \right]_{\text{melt}}. \quad (20)$$

The rate of change in snow density caused by snow compaction is given by

$$\frac{\partial \rho_s}{\partial t} = -\rho_s \left[\frac{1}{\Delta z} \frac{\partial \Delta z}{\partial t} \right]_{\text{total}}. \quad (21)$$

Improving the snow physics

M. Shrestha et al.

Title Page

Abstract

Introduction

Conclusions

References

Tables

Figures

◀

▶

◀

▶

Back

Close

Full Screen / Esc

Printer-friendly Version

Interactive Discussion



2.2.5 Snow albedo

The snow albedo is parameterized using a physically based prognostic snow albedo scheme of the BATS model (Dickinson et al., 1993; Yang et al., 1997). The albedo is computed for VIS and NIR spectral bands with adjustments for illumination angle and snow age. The total snow albedo (α_s) is the weighted average of VIS and NIR albedos, which depends on the spectral ratio of the incident shortwave radiation. VIS and NIR albedos (α_{vis} , α_{nir}) are defined as

$$\begin{aligned}\alpha_{vis} &= \alpha_{vd} + 0.4 \times f_{zen} \times (1 - \alpha_{vd}) \\ \alpha_{nir} &= \alpha_{nird} + 0.4 \times f_{zen} \times (1 - \alpha_{nird}) \\ \alpha_{vd} &= \alpha_{vis0} \times (1 - 0.2 \times f_{age}) \\ \alpha_{nird} &= \alpha_{nir0} \times (1 - 0.5 \times f_{age})\end{aligned}, \quad (22)$$

where α_{vd} and α_{nird} are the albedos of the diffused shortwave radiation in the VIS and NIR bands, respectively, α_{vis0} (0.95) and α_{nir0} (0.65) represent fresh-snow albedos for the VIS and NIR bands, f_{zen} is the correction term for a solar zenith angle larger than 60° and f_{age} is the snow aging factor accounting for the effect of grain growth due to vapor diffusion and the effect of dirt and soot. The snow albedo parameterization is very sensitive to α_{vis0} and α_{nir0} . These fresh-snow albedos can be parameterized depending upon the snow type and characteristics of the site. Details of f_{zen} and f_{age} can be found in Dickinson et al. (1993); Yang et al. (1997).

3 Dataset

Two SnowMIP alpine sites, namely Col de Porte (CDP) in the French Alps and Weissfluhjoch (WFJ) in the Swiss Alps, are selected to evaluate the veracity of WEB-DHM-S in two different climates. Details about data and site characteristics are discussed here and a summary is given in Table 2.

HESSD

7, 3481–3519, 2010

Improving the snow physics

M. Shrestha et al.

Title Page

Abstract

Introduction

Conclusions

References

Tables

Figures

◀

▶

◀

▶

Back

Close

Full Screen / Esc

Printer-friendly Version

Interactive Discussion



3.1 Col de Porte

CDP is a mid-range elevation site at 1340 m a.m.s.l., located in the northern French Alps (45.3° N, 5.77° E) and managed by Météo-France. The site is characterized by flat topography with loamy soil covered with short grass. The soil generally does not freeze. Meteorological and snow-related data for the two snow seasons of 1996–97 and 1997–98 are available through SnowMIP but only data for 1997–98 are used in this study. Figure 2a shows the selected meteorological dataset for 1997–98. Continuous snow cover is recorded from the end of November to early May. Winter air temperatures are not particularly low and rainfall can occur at anytime during the snow season. The site is not windy and is relatively humid. Meteorological forcing data comprise hourly measurements of air temperature, relative humidity, wind speed, precipitation amount, the snow/rain index and downward shortwave and longwave radiation. Evaluation data comprise hourly observations of snow surface temperature from a downward-looking radiometer, hourly observations of snow depth from an ultrasonic sensor supported by weekly snow course observations of the SWE and snow depth, and the daily total of bottom runoff from a 5 m² lysimeter protected from lateral flow. The vegetation coverage parameter is set to zero for simulation following Douville et al. (1995). Data from this site have been used to evaluate many SVAT snow schemes (e.g., Brun et al., 1992; Douville et al., 1995; Loth and Graf 1998a; Sun et al., 1999; Essery et al., 1999; Sun and Xue, 2001; Boone and Etchevers, 2001; Strasser et al., 2002; Xue et al., 2003; Essery and Etchevers, 2004; Brown et al., 2006; Li et al., 2009).

3.2 Weissfluhjoch

The WFJ site is a high-elevation site at 2540 m a.m.s.l. with flat topography, located in the eastern Swiss Alps (46.83° N, 9.81° E) and managed by the Swiss Federal Institute for Snow and Avalanche Research. Meteorological and snow-related data for 1992–93 are available through SnowMIP. Figure 2b shows the selected meteorological dataset for 1992–93. The site meteorology is characterized by a cold and dry winter

HESSD

7, 3481–3519, 2010

Improving the snow physics

M. Shrestha et al.

Title Page

Abstract

Introduction

Conclusions

References

Tables

Figures

◀

▶

◀

▶

Back

Close

Full Screen / Esc

Printer-friendly Version

Interactive Discussion



with a longer period of snow cover than is the case for CDP. The average air temperature during the period of continuous snow cover is -2.9°C . Rainfall does not occur from mid-October to mid-May. Snow continuously accumulates from mid-October until mid-April and then melts through May and June owing to strong solar radiation and temperatures above the melting temperature. Although this site is windier than CDP, drifting and blowing effects are weaker (Essery and Etchevers, 2004; Brown et al., 2006). Meteorological forcing data comprise hourly measurements of air temperature, relative humidity, wind speed, precipitation amount, the snow/rain index and downward shortwave and longwave radiation (see Fig. 2b). Evaluation data comprise hourly observations of snow surface temperature from an infrared thermometer, hourly observations of snow depth from an ultrasonic sensor supported by weekly and sometimes biweekly snow pit observations of the SWE and snow depth, daily snow albedo and daily snowmelt runoff. The vegetation coverage parameter is set to zero for simulation. Data from this site have been used in the assessment of many snow models (e.g., Fierz and Lehning, 2001; Lehning et al., 2002; Fierz et al., 2003; Essery and Etchevers, 2004; Etchevers et al., 2004; Brown et al., 2006).

4 Simulation results

The performance of the model is evaluated by comparing the simulated and observed SWE, snow depth, snow surface temperature, snow density, snow albedo and snowmelt runoff. The bias error (BIAS) and root mean square error (RMSE) are used as evaluation criterion for the simulated results and are defined as

$$\text{BIAS} = \frac{1}{n} \sum_{i=1}^n (X_{\text{sim}_i} - X_{\text{obs}_i}), \quad (23)$$

$$\text{RMSE} = \sqrt{\frac{1}{n} \sum_{i=1}^n (X_{\text{sim}_i} - X_{\text{obs}_i})^2}, \quad (24)$$

Improving the snow physics

M. Shrestha et al.

Title Page

Abstract

Introduction

Conclusions

References

Tables

Figures

◀

▶

◀

▶

Back

Close

Full Screen / Esc

Printer-friendly Version

Interactive Discussion



where $X_{sim,t}$ and $X_{obs,t}$ are simulated and observed values at a given time step for n paired simulation and observation values.

4.1 Snow water equivalent

The SWE is one of the most significant variables in hydrological applications as it is a direct measure of the total liquid water available in the snowpack and is used for predicting seasonal discharge. SWE values simulated by WEB-DHM and WEB-DHM-S are compared with weekly and biweekly snow course measurements and are shown in Fig. 3 for both CDP and WFJ sites. The observation values at CDP show that ablation prevailed at mid-March causing the continuous decrease in the SWE and the SWE is increased to about 0.25 m with significant snowfall in mid-April. Although both models are able to simulate the snow accumulation process well, the results show that the SWE is overestimated by both models in the mid-season from late January to mid-February. It is found that WEB-DHM is unable to simulate the seasonal evolution of the SWE during the melting season, whereas WEB-DHM-S describes the evolution of the SWE during the melting season in a very acceptable manner.

At the WFJ site, snow coverage lasts from mid-October to late June (see Fig. 3). The results show that the SWE is underestimated by WEB-DHM in the accumulation season owing to the strong melt simulation in early November, and all the snow has melted by mid-May, whereas the SWE simulated by WEB-DHM-S during accumulation seasons is found to be in good agreement with the observed SWE. However, it is found that the SWE is slightly underestimated during early spring. The results of statistical analysis of the simulation results are presented in Table 3. The RMSE and BIAS are found to be remarkably less for the simulations employing WEB-DHM-S.

4.2 Snow depth

The results of the simulation of hourly snow depth for CDP and WFJ are shown in Fig. 4. The analysis is complemented by the use of weekly and biweekly snow course

Improving the snow physics

M. Shrestha et al.

Title Page

Abstract

Introduction

Conclusions

References

Tables

Figures

◀

▶

◀

▶

Back

Close

Full Screen / Esc

Printer-friendly Version

Interactive Discussion



measurements. The RMSE and BIAS are considerably less for the simulations employing WEB-DHM-S (see Table 3). For the CDP site, although both versions of WEB-DHM can simulate the length of the snow cover well, WEB-DHM is unable to capture the variability of snow cover because it assumes a constant snow density. It cannot reproduce the observed decrease in the snow depth due to compaction even though there is no melting. Hence, the performance of WEB-DHM in simulating snow depth is poor for the WFJ site also due to the effect of constant snow density. This problem is well addressed in WEB-DHM-S, which calculates the snow depth on the basis of the dynamic evolution of snow density. For the WFJ site, the snow depth simulated by WEB-DHM-S is found to be remarkably underestimated from early April to early June. Statistical analysis shows that WEB-DHM has less BIAS than WEB-DHM-S but it does not mean that the WEB-DHM results are good. Indeed, there is a large overestimation of snow depth by WEB-DHM from January to mid-April and a large underestimation from mid-April to late June. In general, WEB-DHM-S is found to simulate the variability in snow depth with the desired accuracy.

4.3 Snow density

An accurate simulation of snow density is required for the calculation of the snow depth and the thermal conductivity of snow. Snow density is indirectly associated with the calculation of the liquid water and ice content, attenuation of shortwave radiation inside the snowpack, heat conduction and the internal energy of the snowpack. For SnowMIP sites, snow density is derived from weekly and biweekly snow course observations of the snow depth and SWE and compared with the simulation results of WEB-DHM-S. As mentioned previously, WEB-DHM cannot simulate the seasonal variation in snow density since the model assumes a constant value throughout the simulation period.

Figure 5 compares the observed snow density and the snow density simulated by WEB-DHM-S, revealing that WEB-DHM-S is able to capture the trend of the seasonal variation in the snow density. At the CDP site, the snow density is overestimated in the mid-season during mid February owing to the overestimation of snowmelt. At the

Improving the snow physics

M. Shrestha et al.

Title Page

Abstract

Introduction

Conclusions

References

Tables

Figures

◀

▶

◀

▶

Back

Close

Full Screen / Esc

Printer-friendly Version

Interactive Discussion



end of the melting season, the observed snow density has increased to 450 kg m^{-3} but the model fails to simulate this event owing to underestimation of the SWE during this period. The model output shows similar characteristics at the WFJ site. Table 2 shows that the performance of WEB-DHM-S is commendable in simulating snow density as the RMSE and BIAS are found to be much less than those for WEB-DHM.

4.4 Snow surface temperature

Snow surface temperature is an important parameter of the land surface energy balance as it plays a vital role in the estimation of exchanges of moisture and heat fluxes between the snow surface and atmosphere. Figures 6 and 7 compare observations of the snow surface temperature and the simulation results of WEB-DHM and WEB-DHM-S for the dataset of the observing period from 3 December 1997 to 3 May 1998 for the CDP site and from 28 October 1992 to 3 May 1993 for the WFJ site, respectively. The results as shown in Figs. 6 and 7 indicate that the simulation performance of WEB-DHM-S is remarkably improved. Indeed, one of the major results of this research is the significant improvement in the snow surface temperature. WEB-DHM has large RMSE and BIAS because the snow surface temperature is calculated as the averaged temperature for a single bulk layer of snow mass, and thus, the nighttime surface temperature is overestimated.

It is found that the RMSE and BIAS considerably reduce to 2.078 and -0.223 K for WEB-DHM-S compared with the RMSE of 3.227 K and BIAS of 1.38 K for WEB-DHM at the CDP site. The results show that WEB-DHM-S still has some cold bias during the night at the CDP site while the model has warm bias during the day and night at the WFJ site (see Figs. 6 and 7). At the WFJ site, the RMSE and BIAS for the simulation results of WEB-DHM-S are 3.098 and 0.76 K, while those for the simulation results of WEB-DHM are 5.699 and 4.136 K. The observed snow surface temperature is available up to 3 May 1993 only whereas continuous snow cover exists till 30 June 1993. The statistical values of BIAS and RMSE for WEB-DHM at the WFJ site will increase

Improving the snow physics

M. Shrestha et al.

Title Page	
Abstract	Introduction
Conclusions	References
Tables	Figures
◀	▶
◀	▶
Back	Close
Full Screen / Esc	
Printer-friendly Version	
Interactive Discussion	



if we analyze the results for the whole snowy period because snow melts out too early in the simulation of WEB-DHM. The scatterplot of simulated snow surface temperature versus observation values for the two models as shown in Fig. 8 demonstrate that the performance of WEB-DHM-S with regard to energy conservation is improved. The squared coefficient correlation (R^2) value for snow surface temperature simulation increases from 0.6 to 0.82 for the CDP site (see Fig. 8a) and from 0.66 to 0.85 for the WFJ site (see Fig. 8b).

4.5 Snow albedo

The snow albedo observed at the WFJ site is used in the model evaluation. There are also snow albedo observations for the CDP site but they are not used in this study as the CDP albedo is underestimated owing to partial obstruction of the sensor's field of view (Etchevers et al., 2004). Fresh snow albedo in the VIS band is calibrated with a factor of 0.95 for the WFJ site and 0.87 for the CDP site. Figure 9 compares the observed daily mean albedo and the simulation results of WEB-DHM and WEB-DHM-S. The simulation results show that WEB-DHM-S is able to capture the seasonal evolution of snow albedo; however, there is a strong bias of 0.1 to 0.15 during the accumulation period, and thus, the results obtained are identical to those obtained using the CLASS model and those available through SnowMIP (Essery and Etchevers, 2004; Etchevers et al., 2004; Brown et al., 2006).

4.6 Snowmelt runoff

Figure 10 compares the observed snowmelt runoff and simulation results of WEB-DHM and WEB-DHM-S at the CDP and WFJ sites. Although the snowmelt runoff measurements for the CDP site are available for the whole simulation period, the runoff comparison is made for the snow season only. The total snowmelt is computed as the sum of melt in each layer which contribute to the surface runoff and infiltration to the soil surface. The timing and total amount of snowmelt runoff is better simulated by

Improving the snow physics

M. Shrestha et al.

Title Page

Abstract

Introduction

Conclusions

References

Tables

Figures



Back

Close

Full Screen / Esc

Printer-friendly Version

Interactive Discussion



WEB-DHM-S than by WEB-DHM. At the CDP site, WEB-DHM-S is found to capture the snowmelt runoff during the accumulation season, mid-ablation season and final melting season. Although the WEB-DHM results also show similar runoff behavior, they include biases during the accumulation season and final melting season. The runoff is greatly underestimated during the accumulation season and is overestimated from the beginning to the middle of April owing to early melt.

At the WFJ site, the observations of snowmelt runoff are available only for a short period (27 April to 7 July 1993) and the simulation results of WEB-DHM-S have far better agreement with the observed runoff pattern than the simulation results of WEB-DHM. A large amount of snowmelt runoff is simulated by WEB-DHM during early April to early May owing to the early melting in the case of WEB-DHM. A substantial improvement in snowmelt runoff simulation is achieved at both sites by WEB-DHM-S with less RMSE and BIAS (see Table 2).

5 Conclusions

This study presented improvements in the snow physics of WEB-DHM by incorporating a three-layer physically based energy balance snowmelt model of SSiB3 and the BATS albedo scheme. WEB-DHM with improved snow physics is termed WEB-DHM-S and was validated at the CDP and WFJ stations for datasets of the SnowMIP project. The three-layer snow model in WEB-DHM-S added more features to the original WEB-DHM to simulate the snow processes more accurately. The snow processes include the variability of snow density, snow depth and SWE, liquid water and ice content in each layer, prognostic snow albedo, diurnal variation in the snow surface temperature, thermal heat due to conduction and liquid water retention.

The simulation results of snow depth, SWE, surface temperature and snowmelt runoff revealed that WEB-DHM-S is capable of simulating the internal snow process more accurately than WEB-DHM, reducing the RMSE and BIAS remarkably. Snow albedo is better parameterized in WEB-DHM-S than in WEB-DHM. Although WEB-

Improving the snow physics

M. Shrestha et al.

Title Page

Abstract

Introduction

Conclusions

References

Tables

Figures



Back

Close

Full Screen / Esc

Printer-friendly Version

Interactive Discussion



DHM-S is capable of capturing an albedo trend similar to that observed, it still has a strong bias of 0.1 to 0.15 in the albedo value during the accumulation period. Therefore, more observational data of albedo should be used to parameterize the snow model with good accuracy. Furthermore, this model was validated at two open sites only, and further work is needed to validate the model in forested areas. Although WEB-DHM-S is only evaluated at a point scale for the simulation of snow processes, this study provides a benchmark for the application of WEB-DHM-S in cold regions in the assessment of the basin-scale SWE, snow coverage and seasonal discharge simulation for water resources management. In future work, WEB-DHM-S can be further coupled with a frozen soil scheme (e.g., Wang et al., 2010) and a glacier model to improve water resources management in alpine river basins.

Acknowledgements. This study was supported by the Ministry of Education, Culture, Sports, Science and Technology of Japan. The authors express deep gratitude to Centre National de Recherches Météorologiques, Météo-France, France, for providing Col de Porte data and the Swiss Federal Institute for Snow and Avalanche Research, Davos, Switzerland, for providing Weissfluhjoch data under the framework of the Snow Model Intercomparison Project.

References

- Anderson, E. A.: A point energy and mass balance model of a snow cover, NOAA Tech. Rep. NWS 19, U.S. Dept. of Commerce, Washington, D.C., 150 pp., 1976.
- Blöschl, G., Kirnbauer, R. and Gutknecht, D.: Distributed snowmelt simulations in an Alpine catchment: 1. Model evaluation on the basis of snow cover patterns, *Water Res. Res.*, 27(12), 3171–3179, 1991.
- Boone, A. and Etchevers, P.: An intercomparison of three snow schemes of varying complexity coupled to the same land surface scheme: Local scale evaluation at an Alpine site, *J. Hydrometeorol.*, 2, 374–394, 2001.
- Boone, A., Habets, F., Noilhan, J., Clark, D., Dirmeyer, P., Fox, S., Gusev, Y., Haddeland, I., Koster, R., Lohmann, D., Mahanama, S., Mitchell, K., Nasonova, O., Niu, G.-Y., Pitman, A., Polcher, J., Shmakin, A.B., Tanaka, K., Van Den Hurk, B., Verant, S., Verseghy, D., Viterbo,

HESSD

7, 3481–3519, 2010

Improving the snow physics

M. Shrestha et al.

Title Page

Abstract

Introduction

Conclusions

References

Tables

Figures

◀

▶

◀

▶

Back

Close

Full Screen / Esc

Printer-friendly Version

Interactive Discussion



Improving the snow physics

M. Shrestha et al.

Title Page

Abstract

Introduction

Conclusions

References

Tables

Figures

◀

▶

◀

▶

Back

Close

Full Screen / Esc

Printer-friendly Version

Interactive Discussion



P. and Yang, Z.-L.: The Rhône–aggregation land surface scheme intercomparison project: An overview, *J. Climate*, 17, 187–208, 2004.

Bowling, L. C., Lettenmaier, D. P., Nijssen, B., Graham, L. P., Clark, D. B., El Maayar, M., Essery, R., Goers, S., Gusev, Y. M., Habets, F., Hurk, B. V. D., Jin, J., Kahan, D., Lohmann, D., Mahanama, S., Mocko, D., Nasonova, O., Niu, G.-Y., Samuelsson, P., Shmakin, A. B., Takata, K., Verseghy, D., Viterbo, P., Xia, Y., Xue, Y. and Yang, Z.-L.: Simulation of high-latitude hydrological processes in the Torne–Kalix basin: PILPS Phase 2(e) 1: Experiment description and summary intercomparisons, *Glob. Planet. Change*, 38, 1–30, 2003.

Brown, R., Bartlett, P., Mackay, M. and Verseghy, D.: Evaluation of snow cover in CLASS for SnowMIP, *Atmos. Ocean.*, 44, 223–238, 2006.

Brun, E., Martin, E., Simon, V., Gendre, C. and Coleou, C.: An energy and mass model of snow cover suitable for operational avalanche forecasting, *J. Glaciol.*, 35, 333–342, 1989.

Brun, E., David, P., Sudul, M. and Brunot, G.: A numerical model to simulate snow-cover stratigraphy for operational avalanche forecasting, *J. Glaciol.*, 38, 13–22, 1992.

Dai, Y., Zeng, X., Dickinson, R. E., Backer, I., Bonan, G. B., Bosilovich, M. G., Denning, A. S., Dirmeyer, P. A., Houser, P. R., Niu, G., Oleson, K. W., Schlosser, C. A., and Yang, Z. L.: The common land model, *Bull. Am. Met. Soc.*, 84, 1013–1023, 2003.

Deardorff, J. W.: Efficient prediction of ground surface temperature and moisture, with inclusion of a layer of vegetation, *J. Geophys. Res.*, 83, 1889–1903, 1978.

Dickinson, R. E., Henderson-Sellers, A., and Kennedy, P. J.: Biosphere-Atmosphere Transfer Scheme (BATS) Version 1e as coupled to the NCAR Community Climate Model, NCAR Tech. Note TN–387 1 STR, 72 pp., 1993.

Douville, H., Royer, J. F., and Mahfouf, J. F.: A new snow parameterization for the Météo-France climate model: Part 1. Validation in stand-alone experiments, *Climate Dyn.*, 12, 21–35, 1995.

Durand, M. and Margulis, S. A.: Feasibility test of multifrequency radiometric data assimilation to estimate snow water equivalent, *J. Hydrometeorol.*, 7, 443–457, 2006.

Essery, R., Martin, E., Douville, H., Fernández, A., and Brun, E.: A comparison of four snow models using observations from an alpine site, *Climate Dyn.*, 15, 583–593, 1999.

Essery, R. and Etchevers, P.: Parameter sensitivity in simulations of snowmelt, *J. Geophys. Res.*, 109, D20111, doi:10.1029/2004JD005036, 2004.

Essery, R., Rutter, N., Pomeroy, J., Baxter, R., Stähli, M., Gustafsson, D., Barr, A., Bartlett, P., and Elder, K.: SnowMIP2 an evaluation of forest snow process simulations, *Bull. Am. Met.*

Improving the snow physics

M. Shrestha et al.

Title Page

Abstract

Introduction

Conclusions

References

Tables

Figures

◀

▶

◀

▶

Back

Close

Full Screen / Esc

Printer-friendly Version

Interactive Discussion



Soc., 90(8), 1120–1135, 2009.

Etchevers, P., Martin, E., Brown, R., Fierz, C., Lejeune, Y., Bazile, E., Boone, A., Dai, Y.-J., Essery, R., Fernandez, A., Gusev, Y., Jordan, R., Koren, V., Kowalczyk, E., Nasonova, N. O., Pyles, R. D., Schlosser, A., Shmakin, A. B., Smirnova, T. G., Strasser, U., Verseghy, D., Yamazaki, T., and Yang, Z.-L.: Validation of the energy budget of an alpine snowpack simulated by several snow models (SnowMIP project), *Ann. Glaciol.*, 38, 150–158, 2004.

Fierz, C. and Lehning, M.: Assessment of the microstructure-based snow-cover model SNOWPACK: thermal and mechanical properties, *Cold Reg. Sci. Technol.*, 33, 123–131, 2001.

Fierz, C., Riber, P., Adams, E. E., Curran, A. R., Föhn, P. M. B., Lehning, M. and Plüss, C.: Evaluation of snow-surface energy balance models in alpine terrain, *J. Hydrol.*, 282, 76–94, 2003.

Hirai, M., Sakashita, T., Kitagawa H., Tsuyuki, T., Hosaka, M., and Oh'izumi, M.: Development and validation of a new land surface model for JMA's operational global model using the CEOP observation dataset, *J. Meteorol. Soc. Jpn.*, 85A, 1–24, 2007.

Jin, J., Gao, X., Sorooshian, S., Yang, Z.-L., Bales, R., Dickinson, R. E., Sun, S. F., and Wu, G. X.: One-dimensional snow water and energy balance model for vegetated surfaces, *Hydrol. Process.*, 13, 2467–2482, 1999a.

Jin, J., Gao, X., Yang, Z.-L., Bales, R. C., Sorooshian, S. and Dickinson, R. E.: Comparative analyses of physically based snow melt models for climate simulations, *J. Climate*, 12, 2643–2657, 1999b.

Jordan, R.: A one-dimensional temperature model for a snow cover, U.S. Army Corps of Engineers, Cold Regions Research and Engineering Laboratory, Special Report, 91–16, 49 pp., 1991.

Lehning, M., Bartelt, P., Brown B. and Fierz, C.: A physical SNOWPACK model for the Swiss avalanche warning Part III: Meteorological forcing, thin layer formation and evaluation, *Cold Reg. Sci. Technol.*, 35, 169–184, 2002.

Li, W. P., Sun, S. F., Wang, B., and Liu, X.: Numerical simulation of sensitivities of snow melting to spectral composition of the incoming solar radiation, *Adv. Atmos. Sci.*, 26(3), 403–412, doi:10.1007/s00376-009-0403-7, 2009.

Liston, G. E. and Elder, K.: A distributed snow-evolution modeling system (SnowModel), *J. Hydrometeorol.*, 7, 1259–1276, 2006.

Loth, B. and Graf, H.-F.: Modeling the snow cover in climate studies. 1. Long-term integrations under different climatic conditions using a multilayered snow-cover model, *J. Geophys. Res.*,

Improving the snow physics

M. Shrestha et al.

Title Page

Abstract

Introduction

Conclusions

References

Tables

Figures

◀

▶

◀

▶

Back

Close

Full Screen / Esc

Printer-friendly Version

Interactive Discussion



103(D10), 11313–11327, 1998a.

Loth, B. and Graf, H.-F.: Modeling the snow cover in climate studies. 2. The sensitivity to internal snow parameters and interface processes, *J. Geophys. Res.*, 103(D10), 11329–11340, 1998b.

5 Luo, L., Robock, A., Vinnikov, K. Y., Schlosser, A. C., Slater, A. G., Boone, A., Braden, H., Cox, P., Rosnay, P. D., Dickinson, R. E., Dai, Y., Duan, Q., Etchevers, P., Henderson-Sellers, A., Gedney, N., Gusev, Y. M., Habets, F., Kim, J., Kowalczyk, E., Mitchell, K., Nasonova, O. N., Noilhan, J., Pitman, A. J., Schaake, J., Shmakin, A. B., Smirnova, T. G., Wetzel, P., Xue, Y., Yang, Z.-L., and Zeng, Q.-C.: Effects of frozen soil on soil temperature, spring infiltration, and runoff: results from the PILPS 2(d) experiments at Valdai, Russia, *J. Hydrometeorol.*, 4, 334–351, 2003.

Lynch-Stieglitz, M.: The development and validation of a simple snow model for GISS GCM, *J. Climate*, 7, 1842–1855, 1994.

15 Marks, D., Domingo, J., Susong, D., Link, T., and David, G.: A spatially distributed energy balance snowmelt model for application in mountain basins, *Hydrol. Process.*, 13, 1935–1959, 1999.

Mocko, D. M. and Sud, Y. C.: Refinements to SSiB with an emphasis on snow physics: Evaluation and validation using GSWP and Valdai data, *Earth Interact.*, 5, 1–30, 2001.

20 Rutter, N., Essery, R., Pomeroy, J., Altimir, N., Andreadis, K., Baker, I., Barr, A., Bartlett, P., Boone, A., Deng, H., Douville, H., Dutra, E., Elder, K., Ellis, C., Feng, X., Gelfan, A., Goodbody, A., Gusev, Y., Gustafsson, D., Hellstrom, R., Hirabayashi, Y., Hirota, T., Jonas, T., Koren, V., Kuragina, A., Lettenmaier, D., Li, W.-P., Luce, C., Martin, E., Nasanova, O., Pumpanen, J., Pyles, R., Samuelsson, P., Sandells, M., Schädler, G., Shmakin, A., Smirnova, T., Stähli, M., Stöckli, R., Strasser, U., Su, H., Suzuki, K., Takata, K., Tanaka, K., Thompson, E., Vesala, T., Viterbo, P., Wiltshire, A., Xia, K., Xue, Y., and Yamazaki, T.: Evaluation of forest snow process models (SnowMip2), *J. Geophys. Res.*, 114, D06111, doi:10.1029/2008JD011063, 2009.

25 Sellers, P. J., Randall, D. A., Collatz, G. J., Berry, J. A., Field, C. B., Dazlich, D. A., Zhang, C., Collelo, G. D. and Bounoua, L.: A revised land surface parameterization (SiB2) for atmospheric GCMs, Part I: Model Formulation, *J. Climate*, 9, 676–705, 1996.

30 Slater, A. G., Schlosser, C. A., Desborough, C. E., Pitman, A. J., Henderson-Sellers, A., Robock, A., Vinnikov, K. Y., Mitchell, K., Boone, A., Braden, H., Chen, F., Cox, P. M., Rosnay, P. de, Dickinson, R. E., Dai, Y.-J., Duan, Q., Entin, J., Etchevers, P., Gedney, N., Gusev, Y.

Improving the snow physics

M. Shrestha et al.

Title Page

Abstract

Introduction

Conclusions

References

Tables

Figures

◀

▶

◀

▶

Back

Close

Full Screen / Esc

Printer-friendly Version

Interactive Discussion



- M., Habets, F., Kim, J., Koren, V., Kowalczyk, E., Nasonova, O. N., Noilhan, J., Schaake, J., Shmakin, A. B., Smirnova, T. G., Verseghy, D., Wetzel, P., Xue, Y., Yang, Z.-L., and Zeng, Q.: The representation of snow in land surface schemes: Results from PILPS 2(d), *J. Hydrometeorol.*, 2, 7–25, 2001.
- 5 Smirnova, T. G., Brown, J. M., Benjamin, S. G., and Kim, D.: Parameterization of cold-season processes in the MAPS land-surface scheme, *J. Geophys. Res.*, 105(D3), 4077–4086, 2000.
- Strasser, U., Etchevers, P., and Lejeune, Y.: Inter-comparison of two snow models with different complexity using data from an alpine site, *Nordic Hydrol.*, 33(1), 15–26, 2002.
- Sud, Y. C. and Mocko, D. M.: New snow-physics to complement SSiB: Part I. Design and
10 evaluation with ISLSCP initiative I datasets, *J. Meteorol. Soc. Jpn.*, 77(1B), 335–348, 1999.
- Sun, S. F., Jin, J., and Xue, Y.: A simple snow-atmosphere-soil transfer model, *J. Geophys. Res.*, 104(D16), 19587–19597, 1999.
- Sun, S. and Xue, Y.: Implementing a new snow scheme in Simplified Simple Biosphere Model, *Adv. Atmos. Sci.*, 18, 335–354, 2001.
- 15 Sun, W.-Y. and Chern, J.-D.: Validation of a one-dimensional snow-land surface model at the sleepers river watershed, *Boundary-Layer Meteorol.*, 116, 95–115, 2005.
- Tarboton, D. G. and Luce, C. H.: Utah Energy Balance Snow Accumulation and Melt Model (UEB), Computer model technical description and users guide, Utah Water Research Laboratory and USDA Forest Service Intermountain Research Station, Logan, 63 pp., 1996
- 20 Verseghy, D. L.: CLASS – a Canadian land surface scheme for GCMs: I. Soil model, *Int. J. Climatol.*, 11, 111–133, 1991.
- Waliser, D., Kim, J., Xue, Y., Chao, Y., Eldering, A., Fovell, R., Hall, A., Li, Q., Liou, K., McWilliams, J., Kapnick, S., Vasic, R., Sale, F. De and Yu, Y.: Simulating the cold season snowpack: The impact of snow albedo and multi-layer snow physics, California Climate Change Center Report, CEC-500-2009-030-D, 2009.
- 25 Wang, L., Koike, T., Yang, K., Jackson, T. J., Bindlish, R. and Yang, D.: Development of a distributed biosphere hydrological model and its evaluation with the Southern Great Plains Experiments (SGP97 and SGP99), *J. Geophys. Res.*, 114, D08107, doi:10.1029/2008JD010800, 2009a.
- 30 Wang, L., Koike, T., Yang, K., and Yeh, P. J.-F.: Assessment of a distributed biosphere hydrological model against streamflow and MODIS land surface temperature in the upper Tone River Basin, *J. Hydrol.*, 377, 21–34, 2009b.
- Wang, L., Koike, T., Yang, D. and Yang, K.: Improving the hydrology of the Simple Biosphere

Improving the snow physics

M. Shrestha et al.

Title Page

Abstract

Introduction

Conclusions

References

Tables

Figures

◀

▶

◀

▶

Back

Close

Full Screen / Esc

Printer-friendly Version

Interactive Discussion



Model 2 and its evaluation within the framework of a distributed hydrological model, *Hydrol. Sci. J.*, 54(6), 989–1006, 2009c.

Wang, L., Koike, T., Yang, K., Jin, R., and Li, H.: Frozen soil parameterization in a distributed biosphere hydrological model, *Hydrol. Earth Syst. Sci.*, 14, 557–571, doi:10.5194/hess-14-557-2010, 2010.

Xue, Y., Sellers, P. J., Kinter, J. L., and Shukla, J.: A simplified biosphere model for global climate studies, *J. Climate.*, 4, 345–364, 1991.

Xue, Y., Sun, S., Kahan, D. S., and Jiao, Y.: Impact of parameterizations in snow physics and interface processes on the simulation of snow cover and runoff at several cold region sites, *J. Geophys. Res.*, 108(D22), 8859, doi:10.1029/2002JD003174, 2003.

Yang, D., Herath, S., and Musiak, K.: A hillslope-based hydrological model using catchment area and width functions, *Hydrol. Sci. J.*, 47(1), 49–65, 2002.

Yang, D., Koike, T., and Tanizawa, H.: Application of a distributed hydrological model and weather radar observations for flood management in the upper Tone River of Japan, *Hydrol. Process.*, 18, 3119–3132, 2004.

Yang, Z.-L., Dickinson, R. E., Robock, A. and Vinnikov, K. Y.: Validation of the snow submodel of the Biosphere-Atmosphere Transfer Scheme with Russian snow cover and meteorological observational data, *J. Climate.*, 10, 353–373, 1997.

Yang, Z.-L. and Niu, G.-Y.: The versatile integrator of surface atmospheric processes: Part 1. Model description, *Glob. Planet. Change*, 38, 175–189, 2003.

Zanotti, F., Endrizzi, S., Bertoldi, G., and Rigon R.: The GEOTOP snow module, *Hydrol. Process.*, 18, 3667–3679, 2004.

Improving the snow physics

M. Shrestha et al.

Title Page

Abstract

Introduction

Conclusions

References

Tables

Figures

◀

▶

◀

▶

Back

Close

Full Screen / Esc

Printer-friendly Version

Interactive Discussion



Table 1. Major differences of snow processes in WEB-DHM and WEB-DHM-S.

Description	WEB-DHM	WEB-DHM-S
Snow layer	Single bulk layer	Three snow layers
Snow density	Set as constant (200 kg m^{-3})	Prognostic snow density
Snow depth	5 times snow water equivalent	Prognostic snow depth
Snow thermal conductivity	Same as that of soil	Depends upon snow density
Shortwave radiation	Not transmitted to snow	Transmitted into snow layers
Snow water/ice content	Not calculated	Calculated
Surface energy fluxes	Applied to whole bulk layer	Applied to only top layer.
Snow albedo	Set as constant but decreases while melting empirically	Prognostic snow albedo considering ageing effect and dependence on solar zenith angle
Snow surface temperature	Snow and ground surface have same temperature. Snow surface temperature is the average temperature of bulk snow layer	Snow surface temperature and ground surface temperature are different
Ground surface temperature	Force restore method of Deardorff (1978) – single layer	Heat conduction between bottom snow layer and soil surface is included
Snow cover fraction	Linear function of snow depth	Asymptotic function of snow depth and snow density

Improving the snow physics

M. Shrestha et al.

Table 2. Meteorological characteristics of Col de Porte (CDP) and Weissfluhjoch (WFJ) sites.

Description	Col de Porte (CDP)	Weissfluhjoch (WFJ)
Simulation period	8 Oct 1997 to 20 June 1998	1 August 1992 to 31 July 1993
Mean air pressure (hPa)	840.00	1005.00
Mean air temperature (K)	276.65	272.75
Mean wind speed (ms^{-1})	0.76	2.00
Mean relative humidity (%)	80.00	69.00
Total solid precipitation (mm)	770.00	1213.30
Total liquid precipitation (mm)	604.00	406.90
Mean daily downward shortwave radiation (Wm^{-2})	209.83	305.97
Mean daily downward longwave radiation (Wm^{-2})	291.10	257.66

Title Page

Abstract

Introduction

Conclusions

References

Tables

Figures

◀

▶

◀

▶

Back

Close

Full Screen / Esc

Printer-friendly Version

Interactive Discussion



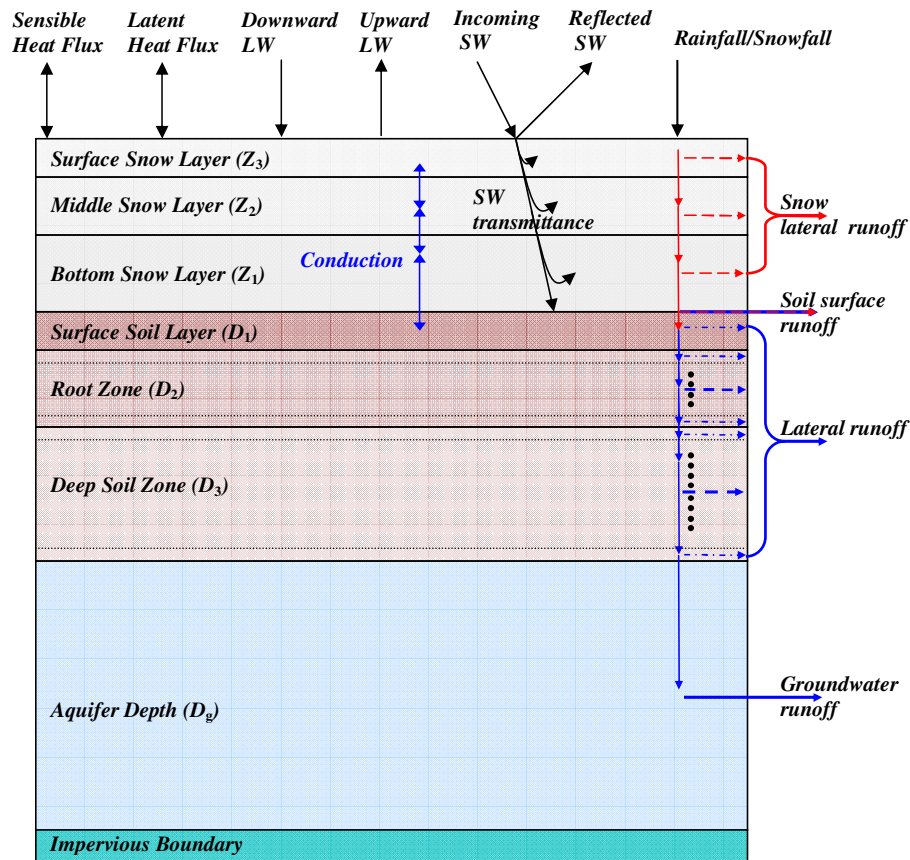


Fig. 1. The soil model coupled with a three-layer snow model as described in WEB-DHM-S.

Improving the snow physics

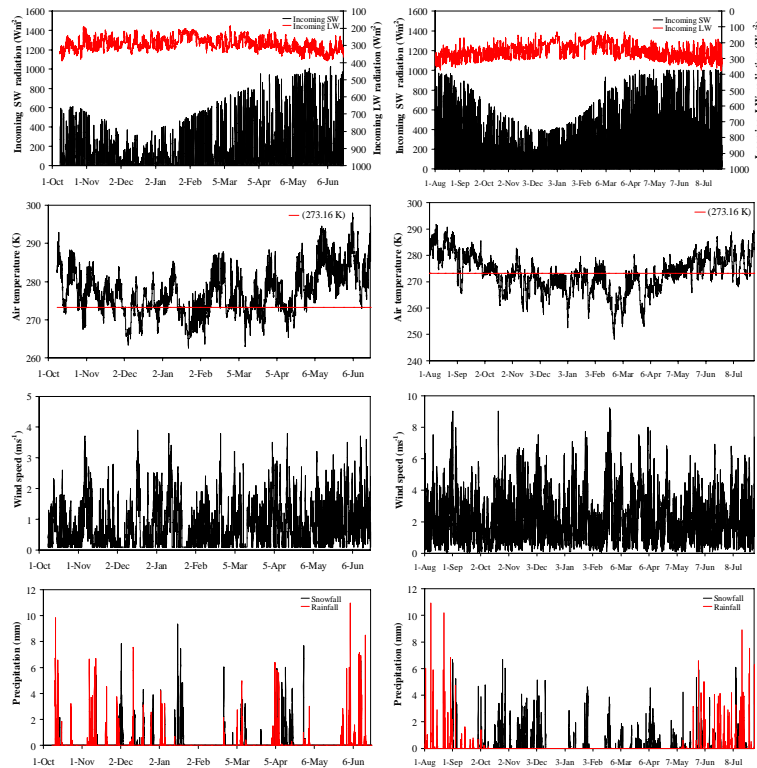
M. Shrestha et al.

Title Page	
Abstract	Introduction
Conclusions	References
Tables	Figures
◀	▶
◀	▶
Back	Close
Full Screen / Esc	
Printer-friendly Version	
Interactive Discussion	



Improving the snow physics

M. Shrestha et al.



(a) Col de Porte (CDP) in 1997–1998

(b) Weissfluhjoch (WFJ) in 1992–1993

Fig. 2. Incoming shortwave and longwave radiations, air temperature, wind speed and snowfall/rainfall for Col de Porte (CDP) from 8 October 1997 to 20 June 1998 **(a)**, and for Weissfluhjoch (WFJ) from 1 August 1992 to 31 July 1993 **(b)**.

Title Page

Abstract Introduction

Conclusions References

Tables Figures

◀ ▶

◀ ▶

Back Close

Full Screen / Esc

Printer-friendly Version

Interactive Discussion



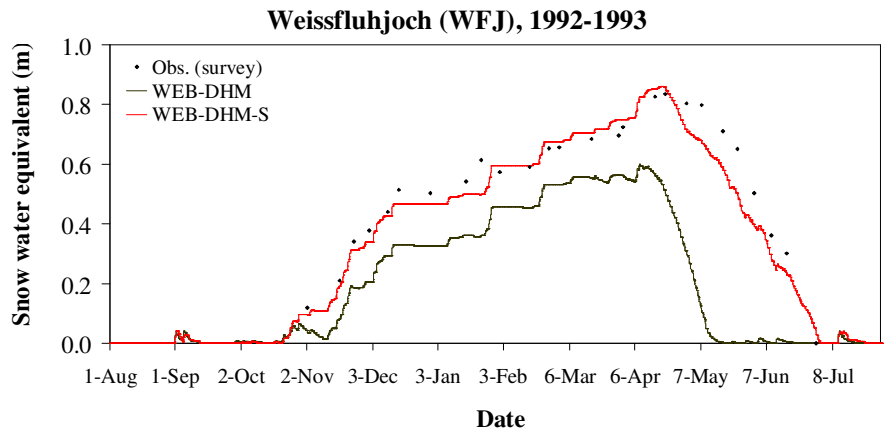
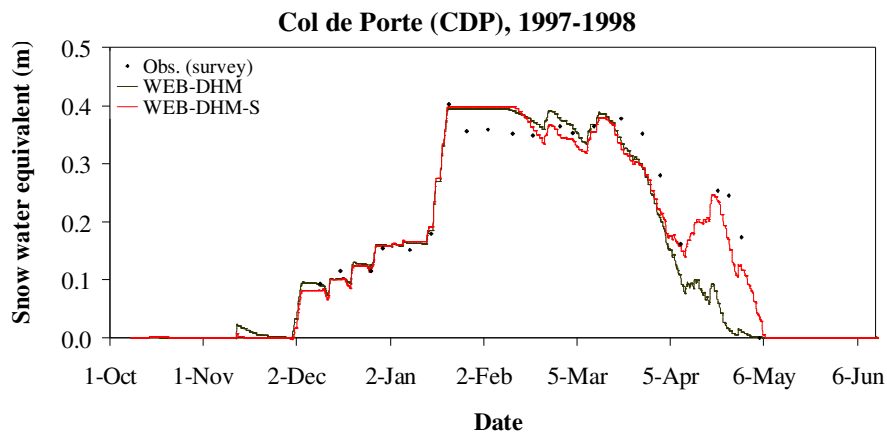


Fig. 3. Comparison of the simulated snow water equivalent (SWE) with the observed snow course measurements for CDP (upper) and WFJ (lower) sites.

Improving the snow physics

M. Shrestha et al.

Title Page	
Abstract	Introduction
Conclusions	References
Tables	Figures
◀	▶
◀	▶
Back	Close
Full Screen / Esc	
Printer-friendly Version	
Interactive Discussion	



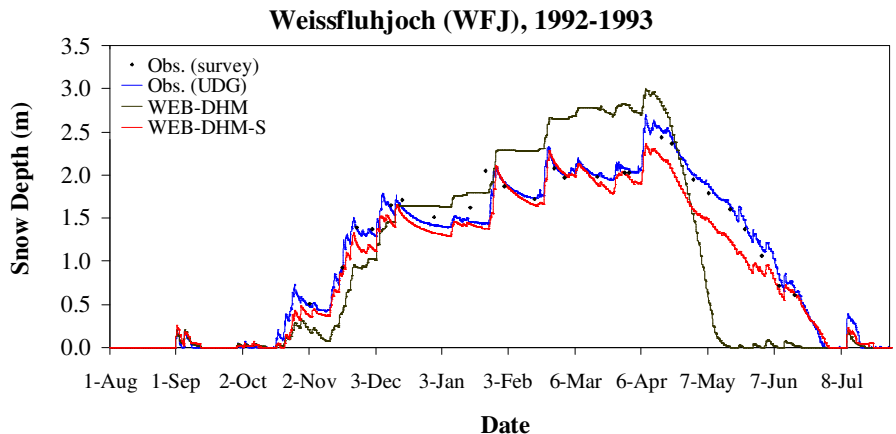
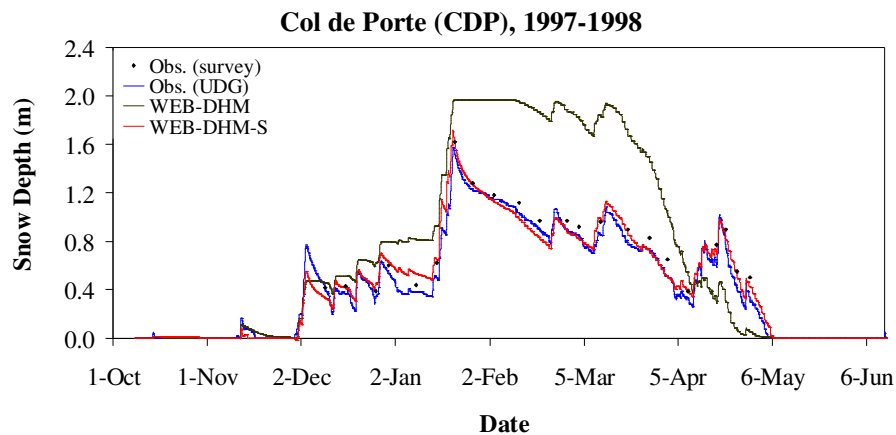


Fig. 4. Comparison of the simulated snow depth with the observed snow depth values from ultrasonic depth gauges (UDG) and snow pit measurements (survey) for CDP (upper) and WFJ (lower) sites.

Title Page	
Abstract	Introduction
Conclusions	References
Tables	Figures
◀	▶
◀	▶
Back	Close
Full Screen / Esc	
Printer-friendly Version	
Interactive Discussion	



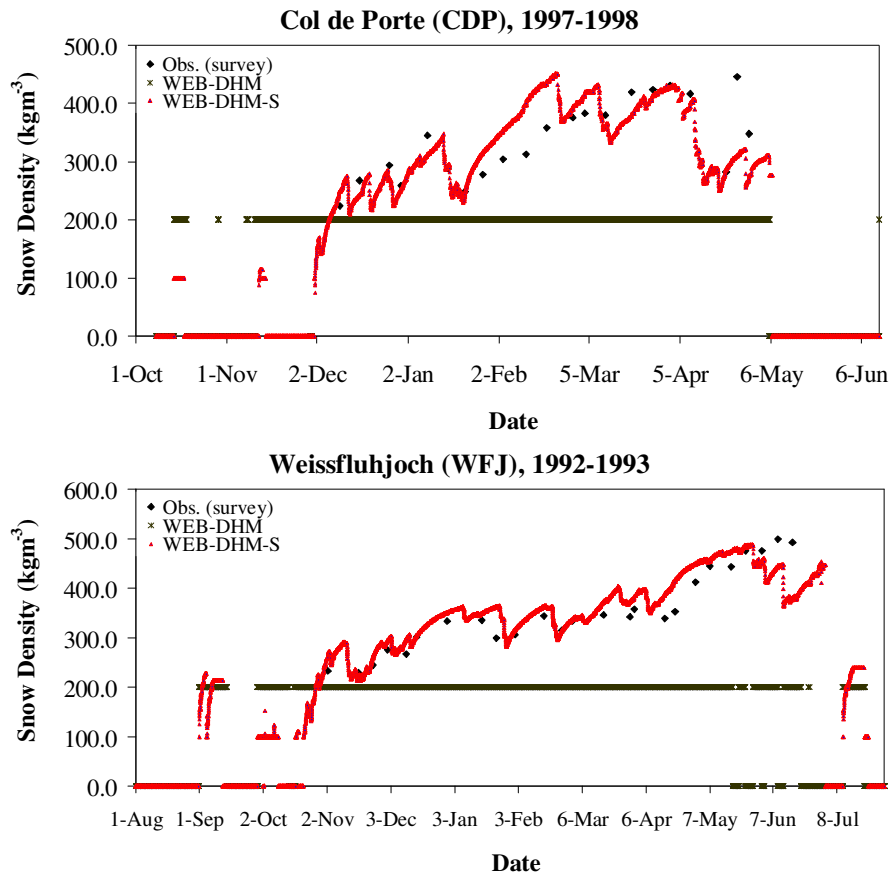


Fig. 5. Comparison of the simulated snow density with the observed snow density derived from observed measurements of SWE and snow depth for CDP (upper) and WFJ (lower) sites.

Title Page

Abstract Introduction

Conclusions References

Tables Figures

◀ ▶

◀ ▶

Back Close

Full Screen / Esc

Printer-friendly Version

Interactive Discussion



Improving the snow physics

M. Shrestha et al.

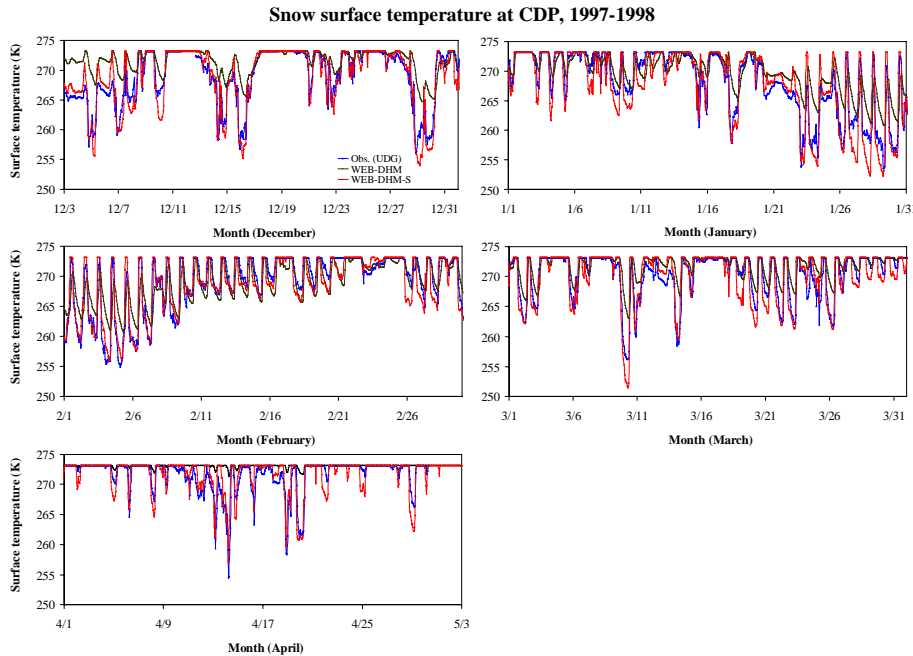


Fig. 6. Comparison of the simulated hourly snow surface temperature with the observed snow surface temperature at CDP site from 3 December 1997 to 3 May 1998.

Title Page

Abstract

Introduction

Conclusions

References

Tables

Figures

◀

▶

◀

▶

Back

Close

Full Screen / Esc

Printer-friendly Version

Interactive Discussion



Improving the snow physics

M. Shrestha et al.

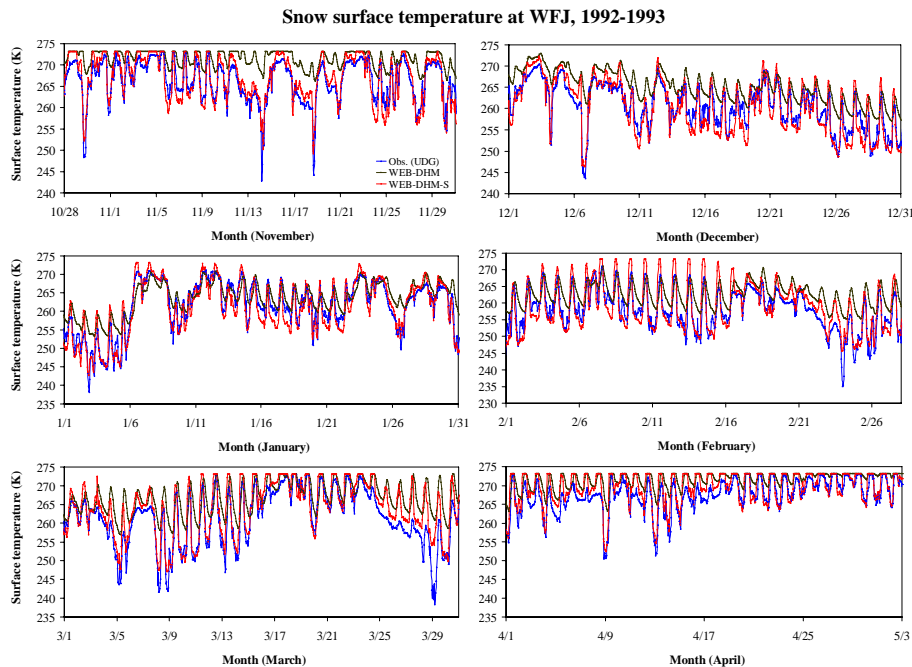


Fig. 7. Comparison of the simulated hourly snow surface temperature with the observed snow surface temperature at WFJ site from 28 October 1992 to 3 May 1993.

[Title Page](#)

[Abstract](#) [Introduction](#)

[Conclusions](#) [References](#)

[Tables](#) [Figures](#)

[◀](#) [▶](#)

[◀](#) [▶](#)

[Back](#) [Close](#)

[Full Screen / Esc](#)

[Printer-friendly Version](#)

[Interactive Discussion](#)



Improving the snow physics

M. Shrestha et al.

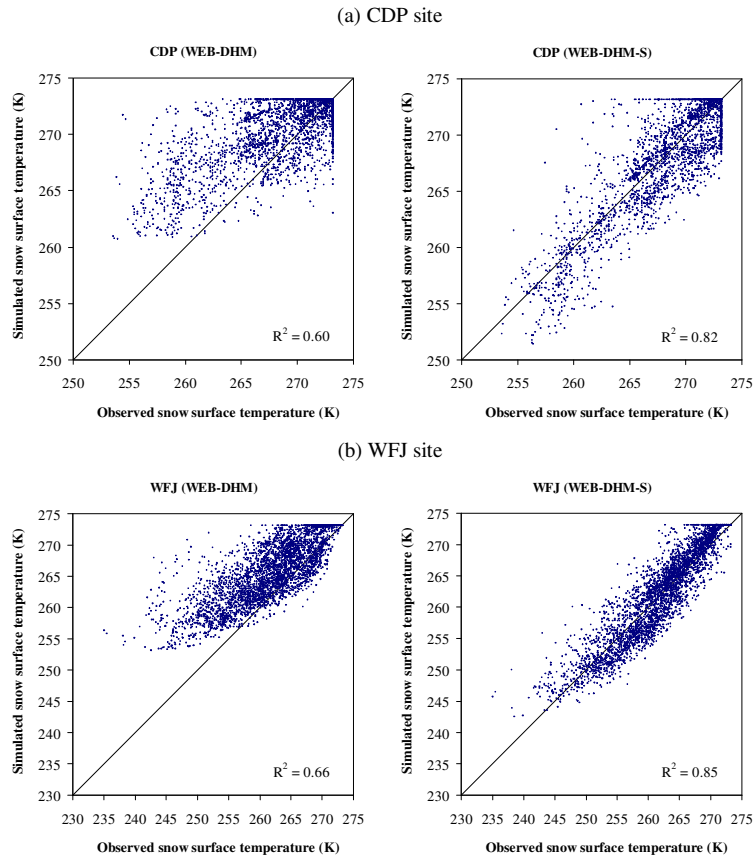


Fig. 8. Scatterplot of the simulated hourly snow surface temperature with the observed snow surface temperature at CDP site from 3 December 1997 to 3 May 1998 **(a)**, and WFJ site from 28 October 1992 to 3 May 1993 **(b)** for WEB-DHM and WEB-DHM-S.

[Title Page](#)[Abstract](#)[Introduction](#)[Conclusions](#)[References](#)[Tables](#)[Figures](#)[I◀](#)[▶I](#)[◀](#)[▶](#)[Back](#)[Close](#)[Full Screen / Esc](#)[Printer-friendly Version](#)[Interactive Discussion](#)

Improving the snow physics

M. Shrestha et al.

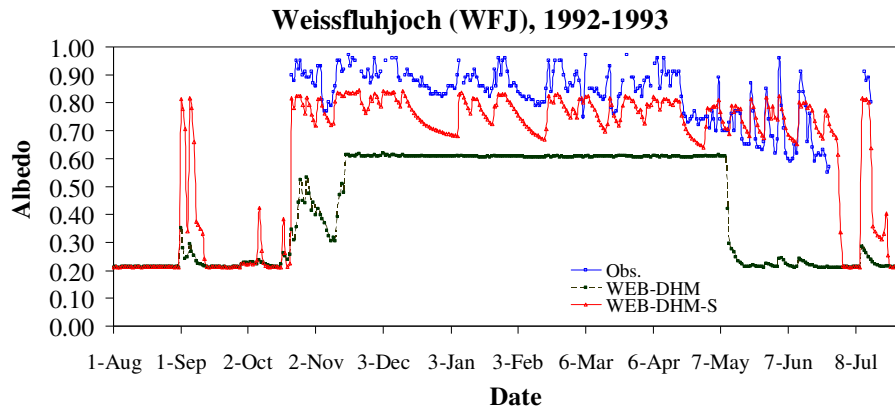


Fig. 9. Comparison of the simulated daily snow albedo with the observed values at WFJ site from 1 August 1992 to 31 July 1993.

[Title Page](#)[Abstract](#)[Introduction](#)[Conclusions](#)[References](#)[Tables](#)[Figures](#)[◀](#)[▶](#)[◀](#)[▶](#)[Back](#)[Close](#)[Full Screen / Esc](#)[Printer-friendly Version](#)[Interactive Discussion](#)

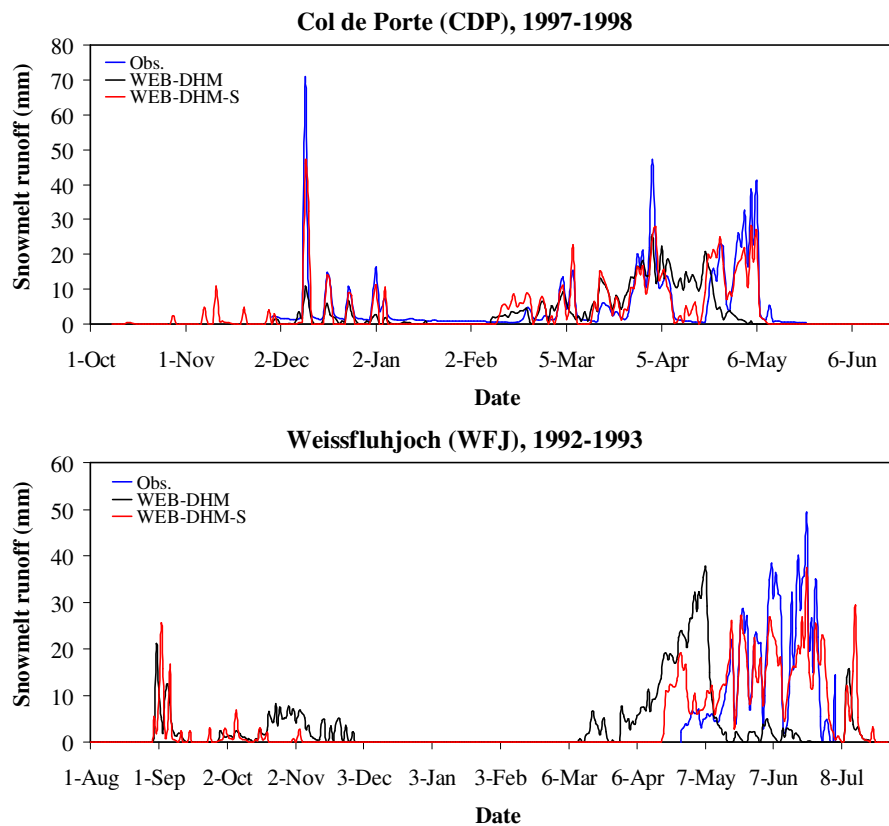


Fig. 10. Comparison of the simulated daily totals of snowmelt runoff with the available observed values at CDP (upper) and WFJ (lower) sites.

Improving the snow physics

M. Shrestha et al.

Title Page

Abstract

Introduction

Conclusions

References

Tables

Figures

◀

▶

◀

▶

Back

Close

Full Screen / Esc

Printer-friendly Version

Interactive Discussion

